Polarization-Insensitive Silicon Microring Modulator for Single Sideband Modulation

Xun Guan, Mingyang Lyu, Wei Shi, and Leslie A. Rusch

IEEE/OSA Journal of Lightwave Technology, (accepted on 15 November 2021)

Doi: 10.1109/JLT.2021.3124467

This article has been accepted for publication in a future issue of this journal, but has not been fully edited. Content may change prior to final publication. Citation information: DOI 10.1109/JLT.2021.3124467, Journal of Lightwave Technology

Polarization-Insensitive Silicon Microring Modulator for Single Sideband Modulation

Xun Guan, *Member, IEEE,*, Mingyang Lyu, Wei Shi, *Member, IEEE,* and Leslie Ann Rusch, *Fellow, IEEE*

***Abstract*—We propose and experimentally demonstrate a polarization-insensitive single sideband modulator based on silicon microring modulators (MRM). The proposed modulator splits and modulates the two orthogonal polarization states of an input laser in a loopback structure, with an on-chip silicon polarization splitter rotator (PSR), overcoming the polarization dependence of the silicon photonic modulator. The IQ configuration of the modulator enables single sideband modulation, thus improving the resistance of the modulated signal to chromatic dispersion and extending the transmission reach. The adoption of an MRM relieves the bandwidth limitation in polarization-diverse versions of SiP Mach-Zehnder modulators (MZM). Our experiments validate the proposed modulator polarization insensitivity and transmission performance.**

***Index Terms*—Wavelength division multiplexing, silicon photonics, optical transmitters, photonic integrated circuits, Electrooptic modulators.**

I. Introduction

SILICON photonics (SiP) is a promising candidate for optical communication, due to its low cost, compactness, and compatibility with complementary metal oxide semiconductor (CMOS) technology [1], [2]. While SiP is being adopted in various optical communications applications, its polarization sensitivity due to mode confinement in a silicon waveguide is a drawback.

Significant effort has been invested into the research on polarization-insensitive SiP transmitters and receivers. At the receiver side, polarization diversity has been realized by incorporating a polarization splitter rotator (PSR), silicon integrated filters and germanium photodiodes [3], [4]. At the transmitter side, polarization diversity in modulators would avoid polarization control or polarization maintaining devices, and facilitate polarization division multiplexing. Various polarization-insensitive modulators have been proposed following different technical routes, including the use of $LiNO_3$, graphene [5], [6], ferro-electric thin film oxide barium titanate ($BaTiO_3$) [7], multilayer-CMOS with indium tin oxide (ITO) [8] and polymer [9]. These solutions are not easily adapted to integration with SiP.

In [10]–[12], a SiP polarization-insensitive modulator is proposed for carrier distribution and remodulation in frequency division multiplexing passive optical networks (FDM-PON) or specifically, at optical network units (ONU). However, this modulator, based on a travelling-wave Mach-Zehnder modulator (TW-MZM), inherently suffers from the bandwidth limitation brought on by the counter propagation of electrical and optical signals. In addition to this, SiP MZM have larger footprint and higher power consumption than SiP microring modulators (MRM) [13]. Consequently, compact and power efficient MRMs are preferred in optical network units (ONUs) [14] and radio access networks [15], [16].

In this paper, we propose a polarization-insensitive SiP MRM modulator, extending the results in our conference presentation [17]. The IQ configuration of this modulator supports single sideband modulation, whose robustness to chromatic dispersion power fading enables longer transmission reach. The proposed modulator shows a higher bandwidth compared to its MZM counterpart, and exhibits high compactness.

The rest of this paper is organized as follows. In section II, theoretical analysis is establishes the polarization insensitivity, single sideband modulation and merits over MZM. Section III introduces our device design, with a fabricated prototype chip that we characterize. Section IV elaborates our experiments using the designed chip to study SSB transmission over different fiber lengths. We also study the polarization insensitivity of the fabricated chip. Section V discusses possible application scenarios of the proposed modulator, and other issues. Section VI concludes the paper.

II. Principle of Operation

A. Polarization insensitivity

Fig. 1 depicts the proposed polarization-insensitive modulator. The input laser at an arbitrary polarization state is coupled into the chip by an edge coupler. In Fig. 1 the upper PSR port outputs the input transverse electrical (TE) component, while the lower port takes the input transverse magnetic (TM) component and converts it and outputs it as TE. The balance of the SiP chip works strictly in TE. The input TE component propagates in a clockwise direction, Fig. 1(a), while the input TM component propagates in a counter-clockwise direction, Fig. 1(b).

Assume the unit input power is split between TE and TM components with percentages α and $1-\alpha$, respectively. The injection laser field across modes is denoted in Jones formalism as

$$|p_{in}\rangle = \begin{pmatrix} \sqrt{\alpha}e^{j\omega t} \\ \sqrt{1-\alpha}e^{j(\omega t+\Delta\varphi)} \end{pmatrix} \quad (1)$$

where $\Delta\varphi$ is the phase difference between the two modes, and ω is the laser angular frequency. We decompose this

The authors are with Centre d'optique, photonique et laser, Département de génie électrique et de génie informatique, Université Laval, Ville de Québec, QC, G1V 0A6, Canada. (e-mail: xun.guan.1@ulaval.ca; mingyang.lyu.1@ulaval.ca, wei.shi@gel.ulaval.ca; leslie.rusch@gel.ulaval.ca).

This article has been accepted for publication in a future issue of this journal, but has not been fully edited. Content may change prior to final publication. Citation information: DOI 10.1109/JLT.2021.3124467, Journal of Lightwave Technology

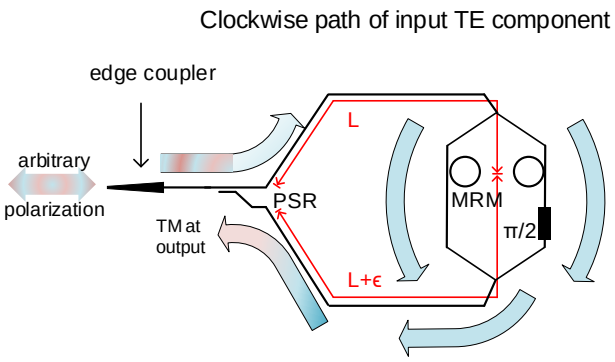

(a)

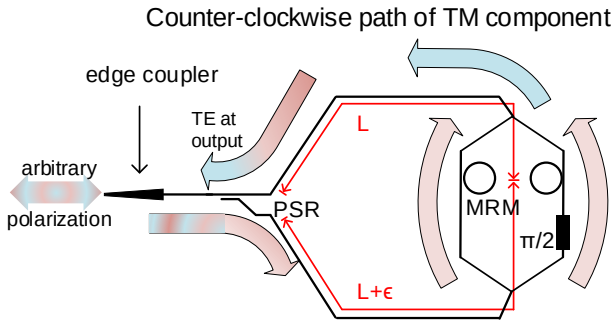

(b)

Fig. 1: Principle of polarization-insensitive single sideband modulator: (a) clockwise propagation of the TE component of input; (b) counter-clockwise propagation of the TM component of input. PSR: polarization splitter rotator; MRM: microring modulator.

unmodulated carrier into the two polarization modes at the input to the PSR, defining

$$|p_1\rangle = \begin{pmatrix} \sqrt{\alpha}e^{j\omega t} \\ 0 \end{pmatrix}, |p_2\rangle = \begin{pmatrix} 0 \\ \sqrt{1-\alpha}e^{j(\omega t+\Delta\varphi)} \end{pmatrix} \quad (2)$$

In Fig. 1(a) we see the TE component of the input, $|p_1\rangle$, propagates on-chip in the clockwise direction.

We assume a symmetric design so that the distance to MRM1 in the clockwise (counter-clockwise) direction is that same as the distance to MRM2 in the clockwise (counter-clockwise) direction. Let L be the propagation length before the MRMs, in the clockwise sense. We allow for deviation from the ideal, with a path length of $L+\epsilon$ for the clockwise return path from the MRMs to the PSR.

Let $A(t)$ and $e^{\varphi(t)}$ be the amplitude and phase, respectively, applied to the MRMs. After on-chip propagation of length L and modulation by the MRM, the modulated clockwise signal is

$$\begin{pmatrix} \sqrt{\alpha}\cdot e^{j(\omega t+\omega\frac{L}{c})}\cdot A(t)e^{\varphi(t)} \\ 0 \end{pmatrix} \quad (3)$$

where c is the speed of light. This signal then propagates and additional length of $L+\epsilon$ before reaching the polarization rotator. The signal is rotated to the TM mode after completing this trajectory. It exits the chip as

$$|p_{1,out}\rangle = \begin{pmatrix} 0 \\ \sqrt{\alpha}\cdot e^{j(\omega t+\omega\frac{2L+\epsilon}{c}+\varphi')}\cdot A(t)e^{\varphi(t)} \end{pmatrix} \quad (4)$$

where φ' is the phase change incurred during the polarization rotation from TE to TM.

The input TM mode $|p_2\rangle$ in Eq. (2) is converted by the PSR to TE mode and becomes

$$|p_2\rangle = \begin{pmatrix} \sqrt{1-\alpha}e^{j(\omega t+\Delta\varphi-\varphi')} \\ 0 \end{pmatrix} \quad (5)$$

This signal propagates in the counter-clockwise direction over a length of $L+\epsilon$. At the MRM the input signal is modulated to become

$$\begin{pmatrix} \sqrt{1-\alpha}\cdot e^{j(\omega t+\omega\frac{L+\epsilon}{c}+\Delta\varphi-\varphi')}\cdot A(t+\frac{\epsilon}{c})e^{\varphi(t+\frac{\epsilon}{c})} \\ 0 \end{pmatrix} \quad (6)$$

Note the new term in both amplitude and phase modulation compared to Eq. (3), $\frac{\epsilon}{c}$, is introduced by the length difference of the two waveguide segments.

The output of counter-clockwise after the modulator is directed over another length L, and travels over the PSR. It does not rotate in polarization by PSR, so the output is

$$|p_{2,out}\rangle = \begin{pmatrix} \sqrt{1-\alpha}\cdot e^{j(\omega t+\omega\frac{2L+\epsilon}{c}+\Delta\varphi-\varphi')}\cdot A(t+\frac{\epsilon}{c})e^{\varphi(t)} \\ 0 \end{pmatrix} \quad (7)$$

Equalizing the two segments via an additional tuning component in the photonic integrated circuit could eliminate this term. Assuming $\epsilon = 0$, the modulated signal in the counter-clockwise direction simplifies to an output of

$$|p_{2,out}\rangle_{\epsilon=0} = \begin{pmatrix} \sqrt{1-\alpha}\cdot e^{j(\omega t+\omega\frac{2L}{c}+\Delta\varphi-\varphi')}\cdot A(t)e^{\varphi(t)} \\ 0 \end{pmatrix} \quad (8)$$

The two modes are combined by the PSR - summing Eq. (4) $\epsilon = 0$ and (8) - to output

$$\begin{aligned} |p_{out}\rangle_{\epsilon=0} &= |p_{1,out}\rangle_{\epsilon=0} + |p_{2,out}\rangle_{\epsilon=0} \\ &= \begin{pmatrix} \sqrt{1-\alpha}\cdot e^{j(\omega t+\omega\frac{2L}{c}+\Delta\varphi-\varphi')}\cdot A(t)e^{\varphi(t)} \\ \sqrt{\alpha}\cdot e^{j(\omega t+\omega\frac{2L}{c}+\varphi')}\cdot A(t)e^{\varphi(t)} \end{pmatrix} \end{aligned} \quad (9)$$

The power output of a photodiode detecting this signal is

$$R = \langle {p_{out}}^* | p_{out}\rangle = |A(t)|^2 \quad (10)$$

which is independent of the input polarization state, α and $\Delta\varphi$.

B. MRM versus MZM

We are interested in SSB generation with either MRM or MZM. Either modulator can use the common method with a pair of Hilbert transform driving the two branches of an IQ modulator [18]. Hence, two modulators with properly matched drive signals directly create SSB without any filtering.

Previous studies [10]–[12] have demonstrated polarization-insensitive travelling-wave MZM modulators. Bidirectional

This article has been accepted for publication in a future issue of this journal, but has not been fully edited. Content may change prior to final publication. Citation information: DOI 10.1109/JLT.2021.3124467, Journal of Lightwave Technology

propagation to achieve polarization diversity has different impact on MZMs and MRMs.

The bidirectional transmission and modulation in a travelling-wave MZM significantly limits its bandwidth. In [10] a silicon MZM with a length of 3.5 mm (a considerably large size for SiP) yielded a narrow bandwidth modulator, due to the counter-propagation of electrical signal and optical signal. The bandwidth could be improved in $LiNbO_3$, but requires a 38 mm phase shifter. The size phase shifter in SiP is unacceptable due to the greater propagation loss, not to mention the integration difficulty.

In contrast, our proposed MRM-based polarization insensitive modulator exploits the easy integration of MRM with lumped electrodes. This circumvents the problems encountered by travelling-wave electrodes. As we will seen in the next section, the MZM in [12] has a 10-dB electrical bandwidth of 6 GHz. Our 10 dB electrical bandwidth is significantly wider at 10.6 GHz. This improvement is largely attributable to the avoidance of travelling-wave electrodes [10]. Our demonstration was limited by the bandwidth of our signal generator and photodiode. With better parameter optimization and novel PN-junction structures for the MRM, its bandwidth can be further boosted, as demonstrated in [19] and [20], without noticeable drawbacks. In our demonstration we highlight the added benefit of using the IQ modulator to achieve single sideband modulation to extend reach in direct detection systems.

III. Device Design, Fabrication and Characterization

We designed and fabricated a chip with the help of AMF Singapore in a 220 nm silicon-on-insulator (SoI) platform. Fig. 2(a) and (b) give the MRM layout in top view and cross-section, respectively. The all-pass PN-junction reverse-bias MRMs have a radius of 10 μm, and a gap of 300 nm between the ring waveguide and straight waveguide. Three doping densities are used in both P and N doping. Fig. 2(c) is a picture of the fabricated MRMs. The PSR, not included in the picture due to limited space, takes the design from [21].

As mentioned previously, the waveguide lengths should be equal from each MRM to the PSR, in both clockwise and counter-clockwise directions. In the design, the two waveguides from the two ends of Mach-Zehnder interferometer structure to the PSR are equalized. To facilitate probing, within the Mach-Zehnder structure we allow a slight location offset between the two MRM. The offset is about 100 μm, leading to a time offset of 0.5 ps. This time offset does not bring discernible impact, which is not surprising as the electrical sampling time is much longer (tens of ps). The MRMs are under-coupled, with a Q factor at about 15,000. The metal heater red-shifts the resonance by about 0.3 nm/mW.

The MRM characterization results are given in Fig. 3. Even though the two MRM are designed to be identical, there could be slight differences in their resonances introduced in fabrication. The red line in Fig. 3(a) shows the spectrum when the resonances of two MRM do not overlap. These resonances can be aligned by thermal control with on-chip heaters, leading to the black curve. Note the different extinction ratios of the MRMs can also be compensated by finely adjusting their reverse bias voltages.

Due to the mismatch in the refractive index of air and the silicon waveguide, there are strong reflections at the edge coupler interface. Without addressing these issues, the MRM spectrum in Fig. 3(a) is unrecoverable. We use refractive index matching gel to alleviate this effect.Some residual fluctuations of the MRM passband are still observable in Fig. 3(a). This residual variation could be further reduced by advanced optical packaging technologies.

One MRM is reverse-biased at -2 V to work in the carrier-depletion mode, while a frequency detuning of 4.5 GHz is set between the laser frequency and the MRM resonance frequency [22], with a 5.5-dB insertion loss [23]. Its S21 parameter is shown in Fig. 3(b), measured with an Agilent N5230 network analyzer. We also reproduce the S21 of the polarization diverse MZM in Fig. 6 of [12] for comparison. We normalize the peaks of the S21 response to one. We show in the inset how the 3 dB, 6 dB and 10 dB bandwidths are determined, and see a clear advantage with the MRM. The MRM modulator sees a 10 dB bandwidth of 10 GHz, vs. 6 GHz for the MZM in [12].

This MRM bandwidth can be increased with a larger detuning frequency, as discussed in [22]. The MRM performance could be further optimized by changing the coupling gap, or with vertical PN-junction[19]; this is beyond the scope of this paper. The upper bandwidth in our demonstration is restricted by the digital-to-analog converter (DAC, Fujitsu Leia, 3-dB bandwidth at 13 GHz) and photodiode (HP 11982A, 3-dB bandwidth at 11 GHz), rather than the MRM bandwidth.

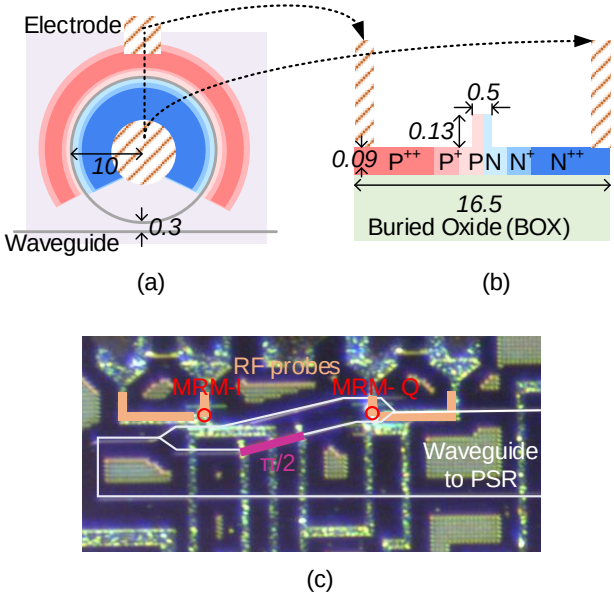

Fig. 2: (a) Layout top view; (b) cross-section of PN junction; (c) A photo of fabricated chip; all dimensions are in μm.

This article has been accepted for publication in a future issue of this journal, but has not been fully edited. Content may change prior to final publication. Citation information: DOI 10.1109/JLT.2021.3124467, Journal of Lightwave Technology

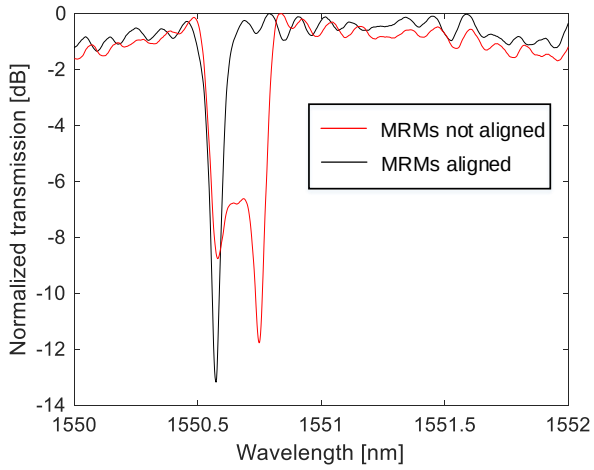

(a)

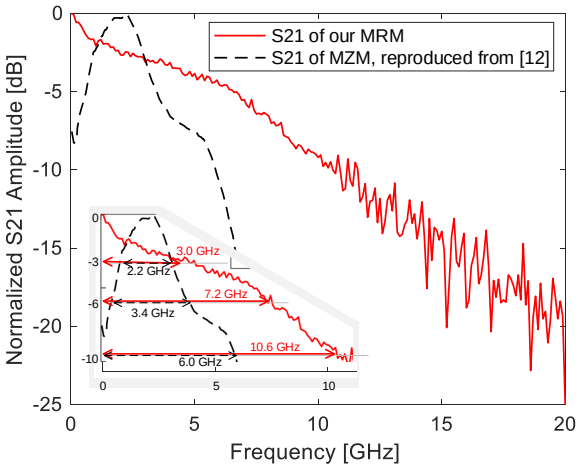

(b)

Fig. 3: (a) Static transmission of MRMs misaligned and aligned; (b) S21 response of an MRM, 1-13 GHz band was selected for modulation.

IV. Experiments

A. Experimental setup

We study our designed modulator in transmission with the setup depicted in Fig. 4(a). Note that all fiber used in the experiment is single-mode fiber (SMF); no polarization maintaining fiber is used. A laser diode (Cobrite DX1, 1550.52 nm) emits laser into a polarization controller/switch (Keysight N7786B), to generate a desired polarization state or to scramble the polarization. The PBS in the dashed box, with the slow-axis as the output, is only used to emulate the polarization-sensitive situation; it is not connected in normal operation. When the PCS sets the polarization state to be aligned to the fast axis, the laser does not transmit over the PBS. A circulator routes the laser into the silicon chip for modulation, while the output is routed to a roll of 20 or 40 km of SMF. After amplification with an erbium-doped fiber amplifier (EDFA), a coupler directs 20% of the signal for monitoring with a high-resolution optical spectrum analyzer (APEX Technologies, AP2043B, 100-MHz resolution). The remaining 80% of the optical power is received with a photodiode (PD, Agilent 11982A with trans-impedance amplifier, 3-dB bandwidth at 11 GHz), and sampled with a real-time oscilloscope (Agilent Infiniium 90000 X-series, 80 GSa/s, 3-dB bandwidth at 33 GHz). The samples are processed with offline digital signal processing.

Fig. 4(b) shows the paths of driving signals to the SiP chip. Two channels of a digital-to-analog converter (DAC, Fujitsu Leia, 64 GSa/s, 3-dB bandwidth at 13 GHz) are amplified and combined with two direct-current power supplies at a -2 V reverse bias, via a bias-T. The two signals drive the MRM, and on-chip heaters align the resonances. We use a heated waveguide to align the phase shifter to $\pi/2$ for IQ modulation.

We use OFDM data modulation with quadrature phase shift keying (QPSK). We use a fast Fourier transform (FFT) size of 1024, and the SSB occupies a frequency band of 1-13 GHz. The 1-GHz guard band is to avoid signal-to-signal interference (SSB), while the band above 13 GHz is avoided due to the poor electrical frequency response of the DAC and photodiode. Because of the MRM non-uniform amplitude response, pre-distortion is applied to equalize the signal-to-noise ratio (SNR) over the modulated subcarriers. Each OFDM symbol includes a 20-sample cyclic prefix (CP). The bit-error ratio (BER) is counted over ten data frames, each with ten OFDM symbols for channel estimation and 230 symbols as payload. With all the overhead deducted, the net bit rate is 22.8 Gbps.

B. SSB versus DSB

We can efficiently combat chromatic-dispersion-induced power fading with SSB. To this end, two signals of a Hilbert-transform pair drive the modulators in the I and Q branches [24]. We demonstrate experimentally that our SSB modulation is effective for different fiber lengths. No polarization controllers are used; polarization diversity is discussed in the next subsection.

The bit error rate (BER) is reported in Fig. 5 for SSB (red, solid lines) and DSB (blue, dotted lines). In DSB, to reach the hard-decision forward error correction (HD-FEC) BER threshold of 3.8×10^{-3}, the received optical power needs to be greater than -8.3 dBm in the back-to-back (B2B) case. With a transmission of 20 km in single-mode fiber, the optical received power required for FEC increases by 1.8 dB to -6.5 dBm. At 40 km, it is impossible to meet the HD-FEC threshold. The degradation of BER performance is due to the power fading of the two sidebands introduced by chromatic dispersion.

For SSB the fading is avoided. All three fiber lengths easily meet the FEC threshold. There is a 1.5 dB power penalty relative to the B2B case. These comparisons clearly show the efficiency of the SiP MRM to generate SSB and achieve robustness to chromatic dispersion.

C. Polarization insensitivity

We examine the polarization insensitivity of the modulator with the experimental setup in Fig. 4. We first set the

This article has been accepted for publication in a future issue of this journal, but has not been fully edited. Content may change prior to final publication. Citation information: DOI 10.1109/JLT.2021.3124467, Journal of Lightwave Technology

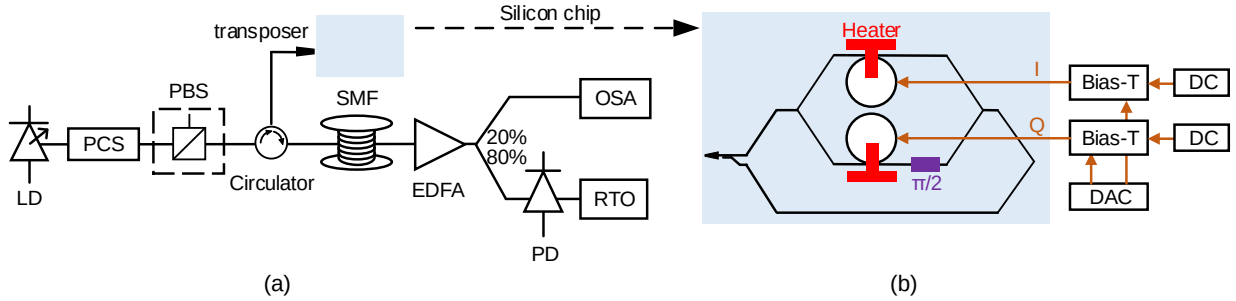

Fig. 4: (a) Experimental setup; (b) SiP chip and driving signals. PCS: polarization controller/switch, PBS: polarization beam splitter, SMF: single-mode fiber, EDFA: erbium-doped fiber amplifier, OSA: optical spectrum analyzer, PD: photodiode, RTO: real-time oscilloscope, DAC: digital-to-analog converter, DC: direct-current power supply. The PBS is only connected when emulating the polarization-sensitive case.

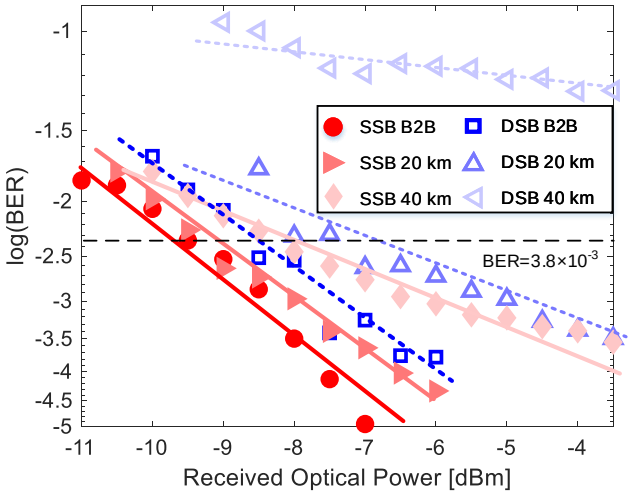

Fig. 5: BER performance of SSB and DSB with different transmission lengths.

depends on the polarization plane of S_2.

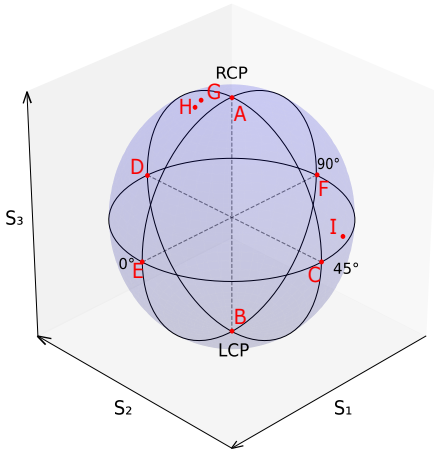

Stokes parameters of A-I

	S1	S2	S3
A	0	0	1
B	0	0	-1
C	0	1	0
D	0	-1	0
E	1	0	0
F	-1	0	0
G	0.16	0.50	0.85
H	0.18	0.56	0.81
I	-0.31	-0.94	-0.16

Fig. 6: Poincaré sphere, linear polarization D-F, circular polarization A-B, and elliptical polarization G-H; Stokes parameters listed in the table.

polarization to several predefined states, states A to H. The states are depicted on the Poincaré sphere in Fig. 7 and their Stokes parameters are given in the accompanying table. The states examined include circular polarization (A and B), linear polarization (C to F), and elliptical polarization (G to I). We record the optical spectrum at the output of the modulator for each input state in the case of no polarization diversity, and with polarization diversity. To emulate the lack of polarization diversity, the PBS in Fig. 4 is inserted and only the TE component of the incoming light is allowed onto a chip. This mimics the SiP responding only to TE.

The results with polarization diversity are given in Fig. 7(a) and (c), while the lack of diversity yields spectra in in Fig. 7(b) and (d). Fig. 7(a) and (c) include the linear and circular polarization states, while the (b) and (d) include the elliptical polarization states, respectively. Figures 7(a) and (c) show almost identical spectra for all input polarizations. Clearly the polarization diversity is effective. For the non-polarization-diverse case we spectra is severely affected. In Fig. 7(b) comparing states C and D shows that the modulation strongly

The polarization insensitivity is further experimentally studied by dynamically scrambling the polarization state with a PCS. We examine three different scrambling speeds: 70.875°/s, 5670°/s and 141750°/s. In Fig. 8 we report the BER of polarization insensitive (A1 to A3, circle, right triangle and diamond markers) and polarization sensitive cases (square, triangle and left triangle markers). The BER is measured 10 times for each scrambling speed, at one minute time intervals. With polarization diversity, the BER remains below the FEC threshold for all measurements at all scrambling speeds. We have good robustness to a variable polarization state. In comparison, the polarization-sensitive cases have most measurements above the FEC threshold.

The BER in Fig. 8 in the grey section for polarization diverse operation still show some fluctuations, while remaining below the FEC threshold. Nonideal components in the test system exhibits some polarization dependence, especially when the polarization is changing dynamically. In particular, the polarization beam splitter in the setup has different transmission for different polarizations. While the modulation spectrum is

This article has been accepted for publication in a future issue of this journal, but has not been fully edited. Content may change prior to final publication. Citation information: DOI 10.1109/JLT.2021.3124467, Journal of Lightwave Technology

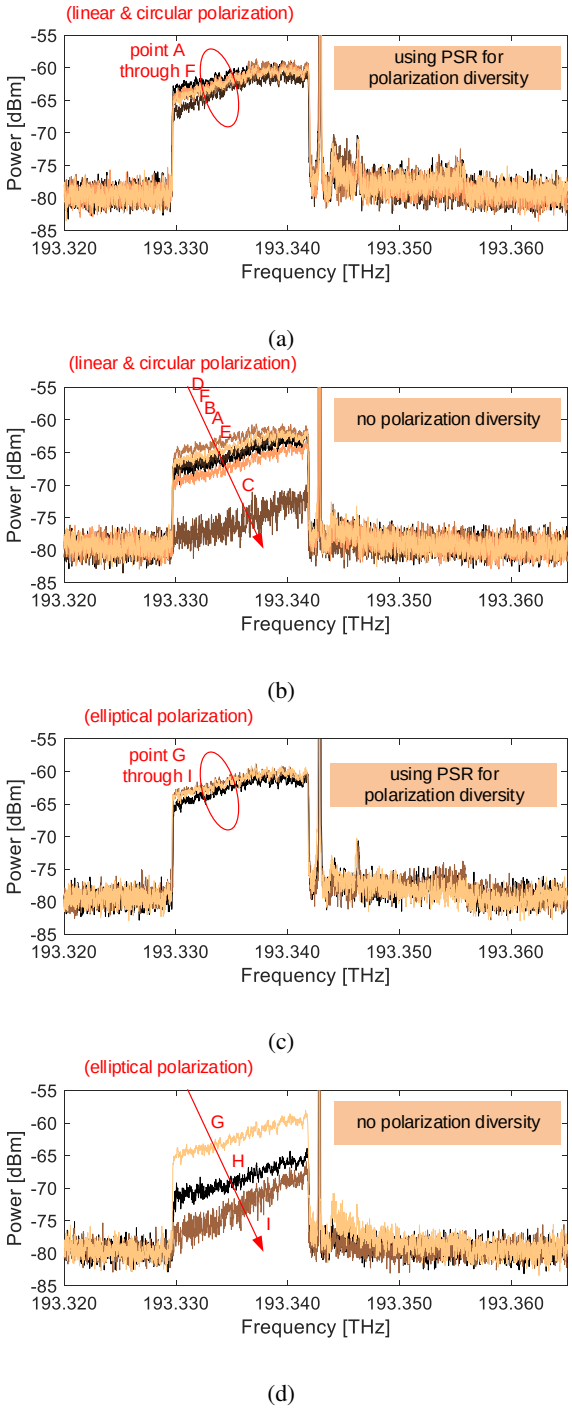

Fig. 7: Modulated spectra of linear and circular polarizations (a) with PSR to achieve polarization insensitivity and (b) without diversity; and modulated spectra of elliptical polarizations (c) with PSR to achieve polarization insensitivity and (d) without diversity.

little affected, this power fluctuation would have an effect on BER.

V. Discussion

We have addressed application scenarios with carrier distribution and remodulation. In addition to the carrier reuse in passive optical networks as in [10], [11], this architecture is also employed with wavelength reuse in radio access networks and radio-over-fiber, as in [25]–[27]. The carrier is subject to polarization rotation during propagation over single mode fiber, with the dynamics of that rotation determined by the ambient environment.

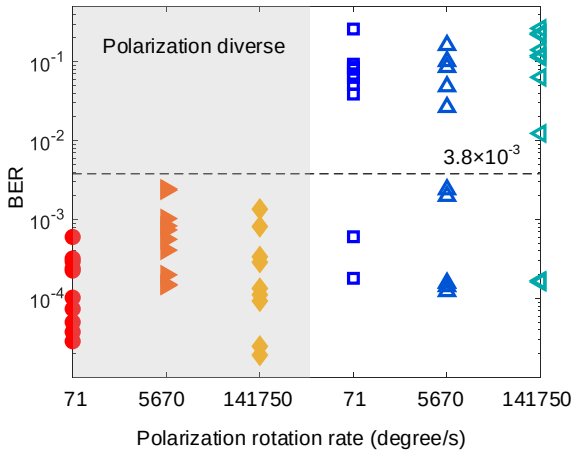

Fig. 8: BER performance of polarization-insensitive (gray shaded results) and polarization-sensitive cases, for different polarization scrambling rates.

We have proposed a polarization-diverse remote modulation using SiP. Another such solution was proposed in [11]. Our solution is predicated on direct detection, while the other solution involved coherent detection. Our solution exploits a wavelength sensitive MRM, while the other is based on a Mach-Zehnder modulator. In section II-B we discussed the advantages and disadvantages of the MRM versus the MZM. We concluded that the MRM offered bandwidth, footprint and power advantages, while the MZM offered greater stability.

The use of direct detection has obvious advantages in cost vis-à-vis coherent detection. In [11] the authors noted that the polarization-diverse SiP with MZM featured the Faraday mirror effect. The structure of the reflected mix of polarization due to this effect could be exploited at the central office. Homodyne detection was achievable, however, polarization multiplexing was precluded. The trade-off in cost and performance when using coherent detection was therefore somewhat diluted. The coherent detection advantages of doubling throughput with polarization multiplexing, as well as the wavelength sensitivity and gain from the use of a local oscillator are lost. Their MZM did not have an IQ structure, so only DSB modulation was examined. The effect of power fading was not addressed.

Finally, we note that the chip in [10], [11] used a 2D grating coupler, while our solution used a edge coupler with a polarization splitter and rotator. The edge coupler can achieve greater coupling efficiency, but requires more complex packaging [28]. As technology evolves, either solution could be adopted in our chip subsystem.

VI. Conclusion

We have proposed a polarization-insensitive SSB modulator, consisting of a PSR and two microring modulators in an MZI configuration. We validate the polarization insensitivity of our design via theoretical analysis and experiments with a fabricated prototype SiP chip. The transmission over several lengths of fiber shows the effectiveness of the MRM generated SSB modulation over DSB modulation. This modulator facilitates low-complexity, low-cost transmitter structures, and enables carrier distribution and reuse for passive optical networks and radio access networks.

Acknowledgement

We would like to thank Ms. Nathalie Bacon, Mr. Simon Levasseur and Mr. Nelson Landry for their technical support. We recognmize CMC Microsystems for the multiproject wafer run. We also acknowledge Telus Communications Inc. and Natural Sciences and Engineering Research Council (NSERC) Canada for their funding support.

References

[1] P. Dong, "Silicon photonic integrated circuits for wavelength-division multiplexing applications," *IEEE Journal of Selected Topics in Quantum Electronics*, vol. 22, no. 6, pp. 370–378, 2016.

[2] W. Shi, Y. Tian, and A. Gervais, "Scaling capacity of fiber-optic transmission systems via silicon photonics," *Nanophotonics*, vol. 9, no. 16, pp. 4629–4663, 2020.

[3] H. Fukuda, K. Yamada, T. Tsuchizawa, T. Watanabe, H. Shinojima, and S.-i. Itabashi, "Silicon photonic circuit with polarization diversity," *Optics express*, vol. 16, no. 7, pp. 4872–4880, 2008.

[4] A. H. Park, H. Shoman, M. Ma, S. Shekhar, and L. Chrostowski, "Ring resonator based polarization diversity WDM receiver," *Optics express*, vol. 27, no. 5, pp. 6147–6157, 2019.

[5] M. K. Shah, R. Lu, D. Peng, Y. Ma, S. Ye, Y. Zhang, Z. Zhang, and Y. Liu, "Graphene-assisted polarization-insensitive electro-absorption optical modulator," *IEEE Transactions on Nanotechnology*, vol. 16, no. 6, pp. 1004–1010, 2017.

[6] X. Hu and J. Wang, "Design of graphene-based polarization-insensitive optical modulator," *Nanophotonics*, vol. 7, no. 3, pp. 651–658, 2018.

[7] P. Tang, D. Towner, A. Meier, and B. W. Wessels, "Low-voltage, polarization-insensitive, electro-optic modulator based on a polydomain barium titanate thin film," *Applied physics letters*, vol. 85, no. 20, pp. 4615–4617, 2004.

[8] X. Qiu, X. Ruan, Y. Li, and F. Zhang, "Multi-layer MOS capacitor based polarization insensitive electro-optic intensity modulator," *Optics express*, vol. 26, no. 11, pp. 13902–13914, 2018.

[9] A. Donval, E. Toussaere, R. Hierle, and J. Zyss, "Polarization insensitive electro-optic polymer modulator," *Journal of Applied Physics*, vol. 87, no. 7, pp. 3258–3262, 2000.

[10] S. Menezo, B. Charbonnier, G. B. De Farias, D. Thomson, P. Grosse, A. Myko, J.-M. Fedeli, B. B. Bakir, G. Reed, and A. Lebreton, "Reflective silicon Mach Zehnder modulator with Faraday rotator mirror effect for self-coherent transmission," in *2013 Optical Fiber Communication Conference and Exposition and the National Fiber Optic Engineers Conference (OFC/NFOEC)*, pp. 1–3, IEEE, 2013.

[11] S. Menezo, E. Temporiti, J. Lee, O. Dubray, M. Fournier, S. Bernabé, D. Baldi, B. Blampey, G. Minoia, M. Repossi, *et al.*, "Transmitter made up of a silicon photonic IC and its flip-chipped CMOS IC driver targeting implementation in FDMA-PON," *Journal of Lightwave Technology*, vol. 34, no. 10, pp. 2391–2397, 2016.

[12] S. Straullu, P. Savio, G. Franco, R. Gaudino, V. Ferrero, S. Bernabé, M. Fournier, V. Muffato, S. Menezo, B. Charbonnier, *et al.*, "Demonstration of a partially integrated silicon photonics ONU in a self-coherent reflective FDMA PON," *Journal of Lightwave Technology*, vol. 35, no. 7, pp. 1307–1312, 2017.

[13] R. Dubé-Demers, S. LaRochelle, and W. Shi, "Ultrafast pulse-amplitude modulation with a femtojoule silicon photonic modulator," *Optica*, vol. 3, no. 6, pp. 622–627, 2016.

[14] L. Xu, Q. Li, N. Ophir, K. Padmaraju, L.-W. Luo, L. Chen, M. Lipson, and K. Bergman, "Colorless optical network unit based on silicon photonic components for WDM PON," *IEEE Photonics Technology Letters*, vol. 24, no. 16, pp. 1372–1374, 2012.

[15] H. Shao, H. Yu, X. Li, Y. Li, J. Jiang, H. Wei, G. Wang, T. Dai, Q. Chen, J. Yang, *et al.*, "On-chip microwave signal generation based on a silicon microring modulator," *Optics letters*, vol. 40, no. 14, pp. 3360–3363, 2015.

[16] Y. Tong, C.-W. Chow, G.-H. Chen, C.-W. Peng, C.-H. Yeh, and H. K. Tsang, "Integrated silicon photonics remote radio frontend (RRF) for single-sideband (SSB) millimeter-wave radio-over-fiber (ROF) systems," *IEEE Photonics Journal*, vol. 11, no. 2, pp. 1–8, 2019.

[17] X. Guan, M. Lyu, W. Shi, and L. A. Rusch, "Silicon microring modulator with polarization insensitivity," in *European Conference on Optical Communication*, pp. TU4D–6, 2021.

[18] M. Klingspor, "Hilbert transform: Mathematical theory and applications to signal processing," 2015.

[19] J. Sun, M. Sakib, J. Driscoll, R. Kumar, H. Jayatilleka, Y. Chetrit, and H. Rong, "A 128 Gb/s PAM4 silicon microring modulator," in *Optical Fiber Communication Conference*, pp. Th4A–7, Optical Society of America, 2018.

[20] Y. Zhang, H. Zhang, M. Li, P. Feng, L. Wang, X. Xiao, and S. Yu, "200 gbit/s optical PAM4 modulation based on silicon microring modulator," in *2020 European Conference on Optical Communications (ECOC)*, pp. 1–4, IEEE, 2020.

[21] W. D. Sacher, T. Barwicz, and J. K. Poon, "Silicon-on-insulator polarization splitter-rotator based on TM0-TE1 mode conversion in a bi-level taper," in *CLEO: Science and Innovations*, pp. CTu3F–3, Optical Society of America, 2013.

[22] J. Müller, F. Merget, S. S. Azadeh, J. Hauck, S. R. García, B. Shen, and J. Witzens, "Optical peaking enhancement in high-speed ring modulators," *Scientific reports*, vol. 4, no. 1, pp. 1–9, 2014.

[23] X. Guan, W. Shi, and L. A. Rusch, "Ultra-dense wavelength-division multiplexing with microring modulator," *Journal of Lightwave Technology*, vol. 39, no. 13, pp. 4300–4306, 2021.

[24] M. Lyu, Y. Xu, L. A. Rusch, and W. Shi, "Single-Sideband OFDM transmission via a silicon microring IQ modulator," *IEEE Photonics Technology Letters*, vol. 31, no. 2, pp. 145–148, 2018.

[25] A. Kaszubowska, L. Hu, and L. P. Barry, "Remote downconversion with wavelength reuse for the radio/fiber uplink connection," *IEEE Photonics Technology Letters*, vol. 18, no. 4, pp. 562–564, 2006.

[26] Z. Jia, J. Yu, and G.-K. Chang, "A full-duplex radio-over-fiber system based on optical carrier suppression and reuse," *IEEE Photonics Technology Letters*, vol. 18, no. 16, pp. 1726–1728, 2006.

[27] Z. Tang and S. Pan, "A full-duplex radio-over-fiber link based on a dual-polarization Mach-Zehnder modulator," *IEEE Photonics Technology Letters*, vol. 28, no. 8, pp. 852–855, 2016.

[28] R. Marchetti, C. Lacava, L. Carroll, K. Gradkowski, and P. Minzioni, "Coupling strategies for silicon photonics integrated chips," *Photonics Research*, vol. 7, no. 2, pp. 201–239, 2019.